Exploiting mm-Wave Communications to Boost the Performance of Industrial Wireless Networks

S. Saponara, F. Giannetti, G. Anastasi, B. Neri, Department of Information Engineering, University of Pisa, Italy

***Abstract*— This work explores the potentiality of millimeter waves (mmW) as physical layer in industrial wireless networks. Innovative models and a link design method are proposed to achieve reliable communication, at a distance of tens of meters for a single hop, even in harsh environments. By exploiting the worldwide-free band of several GHz, available around 60 GHz, mmW links allow to achieve a performance boosting of up to two orders of magnitude, w.r.t. conventional sub-6 GHz wireless links, in indoor industrial environments. Time slotted channel hopping and frequency-diversity can be implemented with a large number of channels, and with high bit rate (several Mb/s per channel). This allows for robust networking of high data-rate sensors, such as cameras, radars or laser scanners. Featuring a low bit error rate, mmW communication allows for low-latency link and large number of hops in networks with a large radius. Finally, it ensures interference separation from operating frequencies of electrical machines, switching converters, and other industrial wireless networks (e.g., 802.11 or 802.15). Implementation results for key HW blocks in low-cost technologies show the feasibility of mmW communication nodes with low-power and compact size.**

Keywords — Wireless industrial networks, physical layer (PHY), mmW communications, link modeling, HW design

I. INTRODUCTION

An exponential increase of the number of deployed sensors and of the generated data rate is characterizing industrial applications, such as process control, robotized production, logistics, energy and environmental management [1]. There is also a growing use of high data-rate sensors, such as video cameras, radar or laser scanners, to implement advanced tasks including obstacle detection, contactless measurements, production quality check, and alarm systems. So far, wired communications have been preferred to face harsh conditions affecting wireless links in industrial environments, such as Non Line-of-Sight (NLOS) connectivity with occlusion and shadowing and electromagnetic interference (EMI). To reduce the wiring harness, and due to the increasing request of number of connections, bandwidth, flexibility and deployment scalability, several short-range wireless technologies have been proposed [1-4]: ZigBee, Bluetooth (BT), BT Low Energy (BLE), wireless HART, ISA-100.11a. At the physical layer (PHY) they operate around 2.4 GHz, or 5 GHz, or in sub-GHz ISM (Industrial Scientific Medical) band [2-4]. In the same frequency band, enhancements for robust networking in industrial scenarios, such as IEEE 802.15.4e, have been released [4]. However, the limited available bandwidth and/or the strong interference with other services co-existing in the crowded sub-6 GHz band, limit the available bit rate. The number and type of sensors to be deployed are also limited. Moreover, the spectrum allocated to GSM, 3G/4G communications is not freely available. Preliminary works about the use of frequencies higher than 10 GHz for industrial wireless networks (24 GHz in [5, 6], 60 GHz in [7, 8]) have been recently proposed in literature. However, the works in [5-7] are limited to point-to-point link budget analysis for specific applications (intruder alarms, tank level metering and motion detectors). The work in [7] is limited to the propagation loss analysis at 60 GHz, and to the evaluation of the maximum connection distance as a function of transceiver HW parameters and environmental conditions. In the above-mentioned works, issues such as network topology, communication latency, impact of single/multi-hop communication, porting at higher frequencies of channel hopping and of ARQ (Automatic Repeat request) techniques, quality-of-service, are not addressed. The work in [8] discusses, at system-level, the industrial potentiality of mmW, but it lacks details on link budget analysis, implementation issues and medium access control (MAC).

To overcome these limitations, this work proposes some channel models, a link design method, and some MAC techniques to explore the potentiality of mmW for industrial communication. At the state-of-the-art, the use of mmW communication is mainly limited to short-range consumer applications. To this aim, alliances have been established, such as WiGig, promoting IEEE 802.11ad for wireless gigabit internet access, or WirelessHD for high-definition multimedia playing/streaming. So far, these alliances did not consider the combined contribution of key issues, such as multi-path, shadowing, occlusions, NLOS, fading, frequency-selective propagation, which are of fundamental relevance in industrial scenarios. Instead, this work takes into account these issues and shows that, even in harsh conditions, a reliable communication can be obtained over tens of meters (for each hop) with 10 mW of transmitted power (1 nJ/bit at 10 Mb/s).

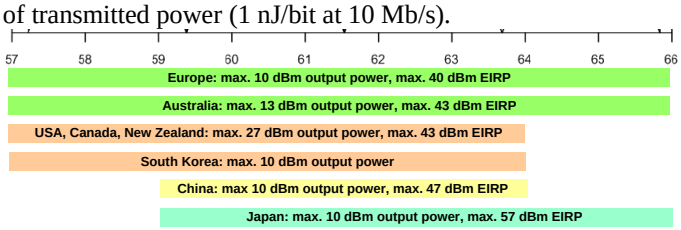

Fig. 1: Worldwide mmW available ISM bands and power limits

At mmW there are up to 9 GHz of bandwidth freely available (from 57 to 66 GHz, see Fig. 1) that can be split in sub-channels. The use of mmW enables the following features:

- Worldwide-unlicensed ISM band of several GHz.
- Wide available band, to be exploited for frequency diversity transmissions and mitigating the effects of the frequency-selective propagation encountered in factory environments, thus yielding more reliable links. For instance, by migrating

the Time Slotted Channel Hopping (TSCH) [4] MAC from 2.4 GHz to 60 GHz a performance increase of two orders of magnitude is obtained, since TSCH could be implemented with 225 channels (of 40 MHz each), providing a bit rate of 10 Mb/s per channel.

- Enhanced spatial separation of neighboring transmitters thanks to extra attenuation of the O_2 absorption band; this enables a higher density [9] of base-stations/access-points.
- Wide separation from the overcrowded and noisy sub-6 GHz frequencies and from EMI originated by electrical machines and power switching converters.

Hereafter, Sections II and III present propagation, signal and noise models in mmW industrial networks under harsh conditions. Efficient occupancy of the mmW spectrum and characterization of frequency-selective fading are discussed, too. Sections IV and V present the communication link design, a trade-off analysis in a simulated environment, and the performance in mesh and star networks. Section VI deals with porting TSCH and ARQ at mmW, and analyses latency in single/multi-hop scenarios. Sections VII and VIII show HW implementation of building blocks and draw some conclusions.

II. MMW FOR INDUSTRIAL NETWORKS PHY

The mmW signals propagate in a quasi-optical fashion, wherein the transmitted (TX) power reaches the receiver (RX) side through LOS path or low-order reflected paths, whilst the contribution of diffracted components is not significant [10]. Around 60 GHz the O_2 absorption peak causes additional attenuation as high as 15 dB/km [11]. In indoor industrial environments, the link distance ranges from a few meters to hundreds of meters, so that the attenuation due to O_2 ranges from few hundredths of dB to a few dB.

A. Path-loss model and multipath channel model

A large number of propagation models for the mmW band, providing the power path-loss (PL) vs. the TX-RX distance d, are available in literature. Most of them [12] are in the form of Eq. (1), where γ is the PL exponent, d_0 is the minimum TX-RX separation for which the model is valid, $\Xi|_{\mathrm{dB}}$ is a zero-mean Gaussian random variable, with standard deviation $\sigma_{\Xi}|_{\mathrm{dB}}$, which takes into account for the long term fading caused by the shadowing phenomenon.

$$\overline{PL}(d)\big|_{\mathrm{dB}} \equiv 10\gamma \log_{10}(d/d_0) + PL(d_0)\big|_{\mathrm{dB}} + \Xi\big|_{\mathrm{dB}} \equiv PL(d)\big|_{\mathrm{dB}} + \Xi\big|_{\mathrm{dB}} \quad (1)$$

To the best of authors' knowledge, in the literature there is a lack of RF measurements in the 60 GHz band in industrial sites and therefore we had to rely mainly on data related to offices and labs. In this paper we use the experimentally-derived parameters for LOS and NLOS indoor propagation at 60 GHz listed in Table I that have been excerpted from [13, 14]. The value of $PL(d_0)$ can be either experimentally derived or theoretically evaluated assuming free-space propagation from the antenna to the boundary of the validity region of the path-loss model, at distance d_0. In the latter case, $PL(d_0) = 68$ dB for a 60 GHz link at d_0 =1 m. All the above cited empirical PL models also include the contribution of the atmospheric (and O_2) attenuation. One of the very few measurements of mmW wireless links in a real industrial machinery is presented in [15], where a small environment enclosed in a metal cabinet is considered (distance within 2 m). The PL model, which is derived from the experimental measurements in [15], turns out similar to that in Eq. (1), and the worst-case values of the relevant parameters are shown to fall within the ranges specified for the models presented in Table I. For example, in [15] the standard deviation $\sigma_{\Xi}|_{\mathrm{dB}}$ is 0.39 dB and $PL(d_0)|_{\mathrm{dB}}$ is 55 dB; the PL exponent measured inside the cabinet is instead overly small (γ =0.02) and it is definitely not applicable to a wide open-space full of obstacles (e.g., a factory environment).

TABLE I. PARAMETERS FOR INDOOR PATH LOSS MODELS AT 60 GHZ

Propagation conditions	Ref.	γ	d_0	$PL(d_0)\|_{\mathrm{dB}}$	$\sigma_{\Xi}\|_{\mathrm{dB}}$
LOS	[13, 15]	0.5–2.5	1 m	Empirical 34–84 dB Free-Space 68 dB	0.14–5.4 dB
	[14]	2.2	1 m	Free-Space 68 dB	2 dB
NLOS	[13]	1.64–5.4	1 m	Empirical 35–86 dB Free-Space 68 dB	1.55–8.6 dB
	[15]	3.3–3.6	1 m	Free-Space 68 dB	up to 9 dB

It is also worthwhile to point out that the LOS and NLOS propagation conditions described in Table I can be easily associated to the "good" and "bad" states, respectively, of the popular Gilbert-Elliott model [16]. However, for the sake of simplicity, in the sequel the link analysis will be separately carried out for the simpler Bernoulli's LOS and NLOS propagation conditions. Though beyond the scope of this paper, the design exploration in the presence of the more complex Gilbert-Elliott model, can be derived from the analytical results presented in Section III.

We assume a multipath channel model, whose baseband complex representation (BBCR) consists of (M+1) paths, each introducing a propagation delay τ_m and a random complex-valued gain $\tilde{A}_m$ ($0 \le m \le M$). For the path m=0 which carries the useful signal, without loss of generality, we assume $\tau_0 = 0$. The multiplicative coefficients $\tilde{A}_m$ of the multipath channel are modelled as independent and identically distributed (i.i.d.) complex-valued random variables, with Rayleigh amplitude and uniform phase, which are the responsible for the short-term fading and are suitably scaled such that $\sum_{m=0}^{M} \mathrm{E}\{|\tilde{A}_m|^2\} \equiv 1$.

B. mmW spectrum occupancy and frequency-selective fading

As shown in Fig. 1, the unlicensed mmW band spectrum around 60 GHz for ISM applications spans 5 GHz in China, 7 GHz in USA, Canada, Japan, South Korea and New Zealand, and a whole 9 GHz in Europe and Australia. All these allocations support a 2.16 GHz channelization. Such a wide portion of spectrum can be used to improve the link in several ways. For example, let assume a maximum bit rate $R_b = 10$ Mb/s for industrial sensors, a Quadrature Phase Shift Keying (QPSK) modulation scheme with coding rate $r = 1/2$,

Notes. $\equiv$ means "by definition"; ~ denotes complex-valued variables; $\mathrm{E}\{\cdot\}$ is the statistical expectation; $\mathrm{Q}(x)$ is the Gauss' integral function; for a bandpass random process $X(t)$, $S_X(f)$ is its PSD, P_X its RF power, $\tilde{X}(t)$ its BBCR.

and Root Raised-Cosine (RRC) pulse shaping with roll-off factor $\alpha = 0.3$. Under these assumptions, the rate of the TX modulation symbols is $R_s = 10$ MBaud and the RF bandwidth is $B_{RF} \equiv (1+\alpha)\, R_s = 13$ MHz. Assuming a 2 MHz-wide guard band on both the sides of the signal spectrum, we end up with a total RF channel occupancy of 15 MHz, yielding a spectral efficiency of 0.67 b/s/Hz. If a spectrum of 9 GHz is freely-available, see Fig.1, we could then potentially allocate up to 600 channels in frequency-division mode, achieving an aggregate throughput of 6 Gb/s. This is, however, an unrealistic performance figure, due to the highly selective behavior of the 60 GHz channel's frequency response, which causes several deep notches across the band, as testified by the experimental results presented in [17]. Actually, in mobile communications, the transmitted radio signal undergoes reflections on surrounding obstacles (buildings, objects, people etc.) and travels via several different paths (a.k.a. *multipath propagation*). Such a type of propagation channel is also termed *time-dispersive* since each of the multipath components experiences a different delay and attenuation. The time-dispersion is measured by the root mean square (RMS) value τ_{RMS} of the multipath channel's delay spread. Multipath components sum up in the receiver and cause a filtering effect where different frequencies of the modulated waveform experience different attenuations and/or phase changes (a.k.a. *frequency-selective* fading [18]).

In the case of mmW signals, the quasi-optical propagation and the high number of reflecting objects, situated around the transmitter and the receiver in indoor industrial environments, dramatically enhance the time-dispersion phenomenon. Experimental results confirm that strong multipath components can arrive at large time delays [19], thus causing a severe frequency-selective behavior of the radio channel. The *coherence bandwidth* B_c, is a fundamental parameter for characterizing the frequency-selective fading and represents the range of frequencies over which the channel lets all spectral components to pass with (approximately) equal gain [18]. This means that any pair of spectral components of the signal that are spaced no more than B_c are statistically correlated, i.e. they are affected by the channel in a similar manner (e.g., both undergo fading or no fading). In detail, the coherence bandwidth is defined as the frequency range over which the correlation function between any pair of spectrum components is always above a given threshold. It is common practice to evaluate the coherence bandwidth assuming a correlation coefficient of 0.5 [20]. Empirical data indicate that B_c and τ_{RMS} are reciprocally related. Assuming a correlation of 0.5, $B_c \approx 1/(5\,\tau_{\mathrm{RMS}})$ [20]. In [12] τ_{RMS} ranges from 5 ns (small-sized lab/offices, 8-12 m^2) to 30 ns (larger labs/offices, 85-105 m^2), and the coherence bandwidth ranges thus from 40 MHz down to 6.6 MHz.

To avoid detrimental in-band distortions (which call for complex countermeasures such as channel estimation and adaptive equalization), the RF signal bandwidth B_{RF} (which depends on the transmitted bit rate) shall not exceed the coherence bandwidth B_c, i.e., $B_{RF} \le B_c$. Under such condition, the signal experiences only flat-fading. Then, wideband signals for high-rate transmissions are much prone to distortions caused by the highly frequency-selective channels (with narrow B_c) that are typically experienced in larger environments. In these cases, the bit rate specifications shall be relaxed down to few Mb/s. As said above, a bit-rate of 10 Mb/s would require $B_{RF} = 13$ MHz. Instead, in the worst case of time-dispersive channels, we must ensure that $B_{RF} \le B_c = 6.6$ MHz, and this reduces the bit rate to 5 Mb/s.

The *coherence time* T_c is a measure of change rapidity of the channel over time, due to movements of people and objects (e.g., robots, vehicles, etc.) in the environment or to movement of the TX/RX antennas, and is given by $T_c \approx 1/(2\, f_D)$, where f_D is the Doppler frequency. For a maximum speed of 10 m/s and a wavelength at 60 GHz of 5 mm, the Doppler frequency is 2 kHz and the coherence time is thus 0.5 ms. In this case we have a "slow fading" since $T_c >> T_s$ (where T_s is the channel symbol interval, 100 µs at 10 Mbaud) and thus, a static channel is experienced. The Doppler shift of 2 kHz, normalized vs. the carrier frequency, leads to a relative shift of $3.33 \cdot 10^{-8}$, with a negligible impact on the link analysis shown below.

C. Frequency-diversity

To improve the robustness of the radio link w.r.t. distortions caused by the frequency-selective fading, some frequency-diversity (FD) technique can be adopted. This approach, which trades-off link throughput and reliability, consists in transmitting the same signal on many suitably spaced (i.e., uncorrelated) channels, and shall be paired with a signal combining technique at the RX side. Depending on the frequency separation, the adopted combining technique and the target outage probability, the adoption of FD over an indoor channel at 60 GHz has been demonstrated to provide a diversity gain ($D_g|_{\mathrm{dB}}$) up to 8 dB [21]. The diversity gain is a measure of how many dB of losses can be saved using the diversity technique for a fixed outage probability. The diversity gain translates into a reduction of the transmit power needed for a given link performance, or, equivalently, in a relaxation of the antenna gain specifications, or in an increase of the link coverage by a factor $10^{D_g|_{\mathrm{dB}}/(10\,\gamma)}$. For example, in LOS ($\gamma = 2.5$) the coverage increase factor is up to 2.

III. Wireless Industrial Link Analysis

According to the above propagation model, Eq. (2) shows the BBCR of the RF signal $R(t)$ at RX side. In Eq. (2) $\Gamma \equiv G_{\mathrm{t}} G_{\mathrm{r}} / \overline{PL}(d)$ is the power gain of the link, with G_{t} and G_{r} the TX and RX antenna gains; $\tilde{S}(t)$ is the BBCR of the RF signal $S(t)$ fed to the TX antenna, whose RF power is P_S; $\tilde{U}(t)$ is the BBCR of the RF useful signal $U(t)$, whose RF power is $P_U \equiv \Gamma\, \mathrm{E}\{|\tilde{A}_0|^2\}\, P_S$; $\tilde{I}(t)$ is the BBCR of the RF multipath interfering component $I(t)$, whose RF power is

$P_I \equiv \Gamma \sum_{m=1}^{M} \mathrm{E}\{|\tilde{A}_m|^2\} P_S$. The amount of multipath is quantified by the "useful-to-multipath power ratio" (known as Rice factor) denoted in (3) as *K*. According to experimental data published in [22, 23], typical values for *K* range from 0.89 dB to 15 dB. From Eq. (3), we get $\mathrm{E}\{|\tilde{A}_0|^2\} = K/(K+1)$, and the RF power of the useful signal can be thus expressed as in Eq. (4), where $\overline{PL}(d) = PL(d)\,\Xi$.

$$\tilde{R}(t) \equiv \overbrace{\sqrt{\Gamma}\tilde{A}_0\tilde{S}(t)}^{\tilde{U}(t)} + \overbrace{\sqrt{\Gamma}\sum_{m=1}^{M}\tilde{A}_m \cdot \tilde{S}(t-\tau_m)}^{\tilde{I}(t)} + \tilde{N}(t) \tag{2}$$

$$K \equiv \frac{P_U}{P_I} = \frac{\mathrm{E}\{|\tilde{A}_0|^2\}}{\sum_{m=1}^{M}\mathrm{E}\{|\tilde{A}_m|^2\}} = \frac{\mathrm{E}\{|\tilde{A}_0|^2\}}{1-\mathrm{E}\{|\tilde{A}_0|^2\}} \tag{3}$$

$$P_U = \left[K/(1+K)\right] P_S G_\mathrm{t}\, G_\mathrm{r} / \overline{PL}(d) \tag{4}$$

Concerning data transmission, the selected modulation and coding scheme (MCS) consists of a modulation with constellation size *W* and an error-correcting code with rate *r*. The bit rate is $R_b \equiv 1/T_b$, where T_b is the bit interval, and the symbol rate is $R_s \equiv 1/T_s$, where T_s is the symbol interval, with $R_b = R_s\, r \log_2 W$. The average useful received RF energy during one bit and one symbol interval are thus $E_b \equiv P_U / R_b$ and $E_s \equiv P_U / R_s$, respectively, with $E_b = E_s/(r\log_2 W)$.

For the noise model, let us consider $\tilde{N}(t)$ as the BBCR of the overall additive white Gaussian noise (AWGN) process $N(t)$, which includes both channel and RX noise contributions. The one-sided RF power spectral density (PSD) of *N*(*t*) is $\eta_0^{(N)} \equiv \mathrm{k}[T_A + (F-1)T_0]$, where $\mathrm{k} = 1.38\cdot 10^{-23}$ J / K, T_A is the noise temperature of the RX antenna, *F* is the noise figure of the RX front-end, and $T_0 = 290$ K. The noise (atmospheric, cosmic, ground-originated) picked up by the antenna is negligible in indoor industrial scenarios, therefore, we let $T_A = 0$ K and $\eta_0^{(N)} = \mathrm{k}(F-1)T_0$. The RF power P_N of the Gaussian noise is $P_N \equiv \eta_0^{(N)} B_N$, where B_N is the one-sided RF noise bandwidth. In case of RRC pulse shaping, $B_N = R_s$. Assuming a large number of i.i.d. components (*M* >> 1), the RF multipath term $I(t)$ is modelled as a further Gaussian process with zero mean, variance P_I, and one-sided RF PSD $\eta_0^{(I)} \equiv P_I / B_N$. The PSD of the overall Gaussian noise is expressed as $\eta_0 \equiv \eta_0^{(N)} + \eta_0^{(I)}$.

In this paper, we pursue the customary approach to the design of digital links in wireless mobile scenarios, which consists in first defining quality-of-service (QoS) requirements. Then, given the signal format and features, the constraints about the HW (e.g., antennas gains, transmitter power, receiver noise figure, etc.), and assuming a proper radio propagation model, the link-budget aims at evaluating the range over which a given source can reliably transmit. The performance metrics considered in this study are: *i*) the maximum required value of the bit error rate (*BER*) at the RX side, denoted as p_req; *ii*) the outage probability, defined as $p_\mathrm{out} \equiv \Pr\{BER > p_\mathrm{req}\}$. The link design must ensure that $BER \le p_\mathrm{req}$, which translates in the condition $E_b/\eta_0 \ge (E_b/\eta_0)_\mathrm{req}$, where $(E_b/\eta_0)_\mathrm{req}$ is the value of E_b/η_0 yielding $BER = p_\mathrm{req}$. For a given PSD noise level η_0, let $(E_b/\eta_0)_\mathrm{req} \equiv (E_b)_\mathrm{req}/\eta_0$, where $(E_b)_\mathrm{req}$ is the required energy per bit, defined as $(E_b)_\mathrm{req} \equiv P_\mathrm{req}/R_b$ where P_req is the required received power, i.e. the receiver's sensitivity, and is expressed as in (5), (6) with $K = P_U/P_I = P_\mathrm{req}/P_I$.

$$\begin{aligned} P_\mathrm{req} &= \eta_0 R_b (E_b/\eta_0)_\mathrm{req} = \\ &= \left\{\mathrm{k}[T_A + (F-1)T_0] + P_\mathrm{req}/(K\,B_N)\right\} R_b (E_b/\eta_0)_\mathrm{req} \end{aligned} \tag{5}$$

$$P_\mathrm{req} = \frac{\mathrm{k}[T_A + (F-1)T_0]}{\left[R_b (E_b/\eta_0)_\mathrm{req}\right]^{-1} - (K\,B_N)^{-1}} \tag{6}$$

With simple algebra, the E_b/η_0 ratio is re-written as in (7), and with further manipulation we get (8), where we introduced the threshold ξ (fading margin). The random attenuation Ξ can exceed the threshold ξ, thus violating the above inequality, and causing an outage event, whose probability can be written as $p_\mathrm{out} = \Pr\{\Xi > \xi\}$. Recalling that the logarithmic attenuation $\Xi|_\mathrm{dB}$ is a zero-mean Gaussian random variable with standard deviation $\sigma_\Xi|_\mathrm{dB}$, the outage probability is $p_\mathrm{out} = \mathrm{Q}(\xi|_\mathrm{dB} / \sigma_\Xi|_\mathrm{dB})$. The link-budget equation, to determine the sustainable bit-rate R_b vs. the link distance *d*, is shown in (9) by re-casting (8) in logarithmic form. From (7), it is apparent that, due to the multipath, E_b/η_0 reaches a floor when the AWGN contribution vanishes. The requirement $E_b/\eta_0 \ge (E_b/\eta_0)_\mathrm{req}$ is met only if *K* is above K_{min}, as in (10).

$$\frac{E_b}{\eta_0} = \frac{K}{\dfrac{(K+1)\,PL(d)\,\Xi\,\eta_0^{(N)}\,R_b}{P_S\,G_\mathrm{t}\,G_\mathrm{r}} + r\log_2 W} \ge \left(\frac{E_b}{\eta_0}\right)_\mathrm{req} \tag{7}$$

$$\Xi \le \xi \equiv \frac{P_S\,G_\mathrm{t}\,G_\mathrm{r}}{(K+1)\,PL(d)\,\eta_0^{(N)}\,R_b}\left(\frac{K}{(E_b/\eta_0)_\mathrm{req}} - r\log_2 W\right) \tag{8}$$

$$\begin{aligned} R_b|_\mathrm{dBHz} &= P_S|_\mathrm{dBm} + G_\mathrm{t}|_\mathrm{dBi} + G_\mathrm{r}|_\mathrm{dBi} - 10\log_{10}(K+1) - PL(d)|_\mathrm{dB} \\ &- \eta_0^{(N)}|_\mathrm{dBm/Hz} - \xi|_\mathrm{dB} + 10\log_{10}\left(\frac{K}{(E_b/\eta_0)_\mathrm{req}} - r\log_2 W\right) \end{aligned} \tag{9}$$

$$K|_\mathrm{dB} \ge K_\mathrm{min}|_\mathrm{dB} \equiv 10\log_{10}(r\log_2 W) + (E_b/\eta_0)_\mathrm{req}|_\mathrm{dB} \tag{10}$$

IV. WIRELESS INDUSTRIAL NETWORK TOPOLOGIES

Using the models derived in Sects. II and III, a link design method will be defined in Section V to evaluate the link performance. To set the link design parameters, two network topologies are considered hereafter, i.e., star and mesh. However, the proposed methodology is general and can be adapted to any network topology. A star topology, shown on the right side of Fig. 2, consists of a number of regular nodes (sensor or actuator devices) and a sink node deployed in the

industrial field. Regular nodes exchange data with the sink node only (no communication among regular nodes). The latter acts as a gateway (GW) to an external network, and may be connected to a remote control server. If the location of regular nodes in the industrial field is fixed and known, they can use directive antennas for communication. Instead, the GW node should use antennas with a large beamwidth whose gain is limited to few dB. In real-world industrial networks, the number of regular nodes is typically limited to few tens [4]. In a star topology all links are single-hop, thus minimizing latency. To allow concurrent communication without conflicts, frequency diversity can be exploited, where each link uses a dedicated channel frequency. A redundant design approach can be pursued where many frequencies are assigned to each link and used in a frequency-hopping fashion (see Section VI). In a star network the coverage area depends on the maximum distance of the link budget analysis in Section V, and it is typically limited. To overcome this, a mesh topology can be used (left side of Fig. 2), wherein each regular node can communicate with other regular nodes, or the GW node, through a path involving multiple hops. With respect to a star network, a mesh topology ensures increased robustness, due to the existence of multiple paths, and allows for a larger coverage area. In a mesh network the maximum end-to-end distance is given by the maximum distance between two directly-communicating nodes multiplied by the maximum number of hops. These improvements are paid in terms of increased latency, since the end-to-end latency is the sum of latencies experienced in the various hops along the path. In a mesh network all regular nodes should avoid too many directive antennas, since each node can receive and retransmit data from its neighbors. Depending on the specific deployment, a large beamwidth of at least 90 degrees is needed. The number of nodes is typically from 10 to 100.

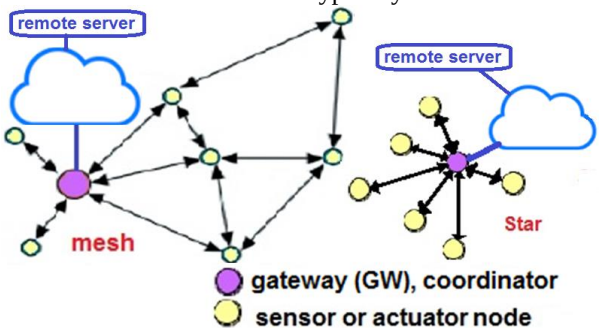

Fig. 2: Mesh (left) and Star (right) topologies

V. MMW LINK PERFORMANCE EVALUATION

The numerical values of PL models and the standard deviation of the shadowing are selected from worst-cases in Table I: for LOS, $\gamma = 2.5$ and $\sigma_{\Xi}\big|_{\text{dB}}$ =5.4 dB; for NLOS $\gamma = 5.4$ and $\sigma_{\Xi}\big|_{\text{dB}}$ =9 dB. Also, $PL(d_0)$ = 68 dB for both cases. The system parameters used for the link analysis of star and mesh topologies, listed in Table II, are based on both state-of-art technology and regulatory issues (e.g. maximum 10 dBm TX power in Europe, up to 27 dBm in US, see Fig. 1). The QoS is specified in terms of the maximum tolerable *BER* at RX side. In the case of industrial applications using video cameras, the wireless links must be designed to ensure $BER \le p_{\text{req}} = 10^{-10}$, as specified in the family of digital video broadcasting (DVB) standards [24]. In Tab. II, G_1 and G_2 represent the gains of the antennas involved in the link, either at TX or RX side. The two network topologies outlined in Sect. IV, differ in the values of the node antenna gain. In the star topology, it is assumed that regular nodes are equipped with a directional antenna (G_1 in Tab. II), while the GW node uses an omnidirectional antenna on the azimuthal plane (G_2 in Tab. II). In the case of mesh topology two options are considered: *i*) a link between two regular nodes, both equipped with large field of view (FOV) antennas (G_1 and G_2 have the same value in this case); *ii*) a link between a regular node, with large FoV antenna, and the GW node with an omnidirectional antenna.

Concerning the MCS, for the sake of simplicity, we focused on single-carrier transmissions with QPSK modulation with concatenated Reed-Solomon (RS) and convolutional encoding for error-correction [24], which also complies with the requirement in (8). Tab. III presents some values of the fading margin, normalized w.r.t. the shadowing deviation $\xi\big|_{\text{dB}} / \sigma_{\Xi}\big|_{\text{dB}}$, and the associated values of the outage probability and of its complement, known as the network uptime. Hereafter, Figs. 3 to 6 show some results of the industrial wireless link analysis, evaluated with the models in Sects. II and III, and the data in Tab. II. Starting from (5) and (6), Fig. 3 shows receiver's sensitivity P_{req}, in dBm, as a function of the bit-rate R_b in kb/s, for F=5dB. Figure 3 shows different curves for different values of the multi-path coefficient K. Figure 4 shows the achievable bit-rate as a function of the distance, considering LOS and NLOS scenarios, and a RX noise figure F from 4 dB to 10 dB.

TABLE II. NUMERICAL VALUES OF THE LINK-BUDGET PARAMETERS

Symbol	Star Topology	Mesh Topology	
Type of nodes involved	Regular node and GW	Two regular nodes	Regular node and GW
$G_1\big\|_{\text{dBi}}$	12 to 18 dBi	5 to 6 dBi	5 to 6 dBi
$G_2\big\|_{\text{dBi}}$	1 to 2 dBi	5 to 6 dBi	1 to 2 dBi
$P_S\big\|_{\text{dBm}}$	5 to 10 dBm		
$F\big\|_{\text{dB}}$	4 to 10 dB		
R_b	1 kb/s to 10 Mb/s		
$K\big\|_{\text{dB}}$	0.89 to 15 dB		
W, r, $(E_b/\eta_0)_{\text{req}}\big\|_{\text{dB}}$, p_{req}, $K_{\min}\big\|_{\text{dB}}$	4, $\frac{1}{2}\cdot\frac{188}{204}$, 5.5 dB, $<10^{-10}$, 5.5 dB		
RF band around 60 GHz	2 to 9 GHz		
p_{out}, $\xi\big\|_{\text{dB}}$	$2.28\cdot10^{-2}$, $2\sigma_{\Xi}\big\|_{\text{dB}}$		

TABLE III. LINK MARGIN AND ASSOCIATED OUTAGE PROBABILITY

$\xi\big\|_{\text{dB}} / \sigma_{\Xi}\big\|_{\text{dB}}$	p_{out}		Network uptime
2.33	10^{-2}	1%	99%
3.08	10^{-3}	0.1%	99.9%
3.72	10^{-4}	0.01%	99.99%
4.26	10^{-5}	0.001%	99.999%

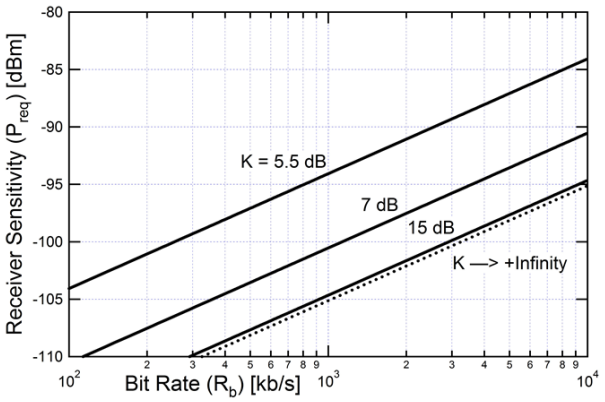

Fig. 3: Required received power *Preq* vs. bit rate

As far as the bit rate, in Tab. II we consider values ranging from few kb/s, typical of industrial sensors [2], up to 10 Mb/s in case of high data-rate sensors [25]. For example, the A35 thermo-camera by FLIR for industrial process control produces images of 356x256 pixels, 8 bits per pixel. Sampling an industrial process at 7.5 fps (15 fps) results in a bit rate of 5 Mb/s (10 Mb/s). In Fig. 4 multipath is considered with K = 7 dB, the TX power is 10 dBm, whereas G_1 = 12 dBi and G_2 = 1.44 dBi. The values for the other link parameters are derived from the analysis in Section III and previous works [22, 24]. The results in Fig. 4 show that, also in the worst–case NLOS environment and considering a feasible value of F=4 dB, reliable links with bit rates of 1 kb/s can be provided up to 20 m. In the most favorable case of LOS conditions, the coverage range grows well beyond hundreds of meters. A bit rate of 5 Mb/s can be transmitted up to 4 m in worst-case NLOS conditions, and to 30 m in LOS conditions. For a bit rate of 10 Mb/s the link distance can be up to 3.5 m and 30 m for NLOS and LOS conditions, respectively. From Fig. 4, we find that at 5 Mb/s the communication distance varies from about 4 m, when F=4 dB, to 3 m, when F=10 dB.

Figure 5 shows that these numerical values can be obtained also in case of a severe multi-path environment with K=5.5 dB, by a proper sizing of the transceiver parameters. Indeed, Fig. 5 shows the link analysis for F=4 dB; the directive TX antenna gain is 18 dBi and the multi-path coefficient K varies from 7.31 dB to the worst case 5.5 dB. Although from experimental data reported in the literature K can vary from 0.89 dB to 15 dB, from Eq. (10) the minimum value ensuring the desired performance ($BER<10^{-10}$, $p_{out}<2.28\cdot10^{-2}$) turns out K_{min} = 5.5 dB. This value is the considered worst case in this Section. For values below K_{min} the connection between two nodes can be still implemented, but the QoS is not guaranteed.

In Fig. 6 the same conditions of Fig. 5 are considered but the EIRP (Equivalent Isotropic Radiated Power), i.e., the sum at TX side of the output power and of the antenna gain, is varied. The EIRP was 22 dBm in Fig. 4 and 28 dBm in Fig. 5. The curves shown in Fig. 6 with EIRP 16 dBm refer to the configuration in Table II, with TX antenna gain 6 dBi and output power 10 dBm. The solid (dashed) lines in Fig. 6 consider a RX antenna gain of 6 (1.44) dBi. As apparent, in NLOS conditions, by setting the EIRP to 16 dBm the link distance is about 20 m at 1 kb/s, 4 m at 5 Mb/s and 3 m at 10 Mb/s. Still in NLOS, by rising the EIRP to 28 dBm the maximum distance grows up to 30 m at 1 kb/s, 6 m at 5 Mb/s and 5 m at 10 Mb/s. This case is representative of star topology with nodes in fixed positions, wherein high-gain directive antennas can be used. In Fig. 6 in LOS scenario the connection distances are one order of magnitude higher than in NLOS. The link design discussed above assumes a very tight *BER* value. If the target application tolerates a higher *BER* (e.g. from 10^{-5} to 10^{-3}), the link budget analysis in Eq. (9) would be aimed at providing a lower RX signal-to-noise ratio (SNR), resulting in a wider coverage, for given HW and bit-rate settings.

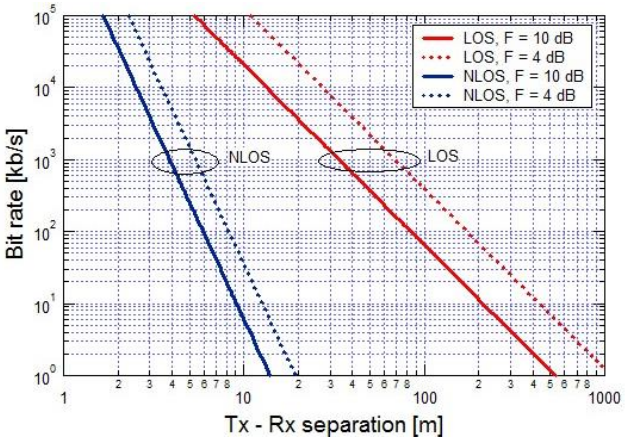

Fig. 4: Bit-rate vs. link distance and noise figure, NLOS/LOS scenario

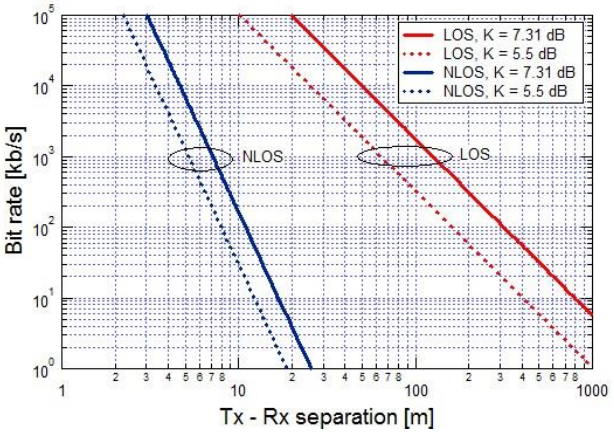

Fig. 5: Bit-rate vs. link distance and multi-path, NLOS/LOS scenario

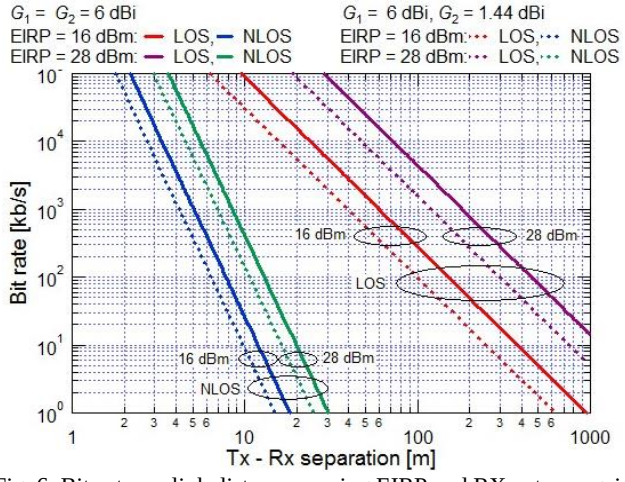

Fig. 6: Bit-rate vs. link distance varying EIRP and RX antenna gain

VI. LINK-LAYER COMMUNICATION PROTOCOLS

The maximum bit rate of 802.15.4e links with a PHY at 2.4 GHz is 250 kb/s only. This is a severe limitation since high-speed industrial wireless networks could be useful when:

i) neighboring nodes are connected by low-rate wired links to a nearby multiplexing unit that sends the aggregate data stream to the remote control server via a wireless link;

ii) nodes contain sensors, such as thermal cameras, generating data streams in the order of 10 Mb/s [25].

Such a need for high bit-rate wireless links can be fulfilled by migrating to the mmW band and exploiting the wide free spectrum available around 60 GHz. Then, let us consider a link in the mmW band using the 802.15.4e packet format whose bit rate is set to 10 Mb/s, with a 40-fold increase of the customary 250 kb/s rate. This entails that the duration of the 128-byte packet considered in [4] reduces 40 times, from 4 ms in [4] to 100 µs in this work. Considering the most favorable limit of a 40 MHz-wide channel from Section II, to avoid selective fading, then the channelization width increases 8 times vs. [4], from 5 MHz to 40 MHz. The 9 GHz-wide available spectrum around 60 GHz can allocate up to 225 channels (9 GHz/40 MHz), yielding a potential support for an aggregate throughput higher than 2 Gb/s (225 channels each at 10 Mb/s). For comparison, the current 802.15.4e standard uses 16 channels, each 5 MHz-wide, over a 80 MHz band and could provide an aggregate throughput of 250 kb/s · 16 = 4 Mb/s.

Since the bit-rate requirements of an industrial network are typically lower than 2 Gb/s, the above 225 channels could be used for redundant communication (e.g., multi-path routing). To improve the link robustness over a time-varying and frequency-selective channel, 802.15.4e features a TSCH scheme (with 16 channels each 5 MHz-wide). Instead, the considered 60 GHz extension of the 802.15.4e could use a TSCH scheme based on 225 channels, with 40 MHz-bandwidth each. In channel hopping, a different channel is selected every time a new packet is transmitted. This requires a fast Phase Locked Loop (PLL), capable of changing the frequency by 40 MHz (or multiples) within a settling time, lower than the packet duration (100 µs at 10 Mb/s for a 128-byte packet in this work). This is not an issue, since in literature PLL circuits for 60 GHz applications, capable of changing the frequency by 500 MHz in less than 1 µs [26], are already available. To ensure robust transmission over the frequency-selective channels of indoor and industrial environments at 60 GHz, the coherence bandwidth shall be greater than the channel width. As discussed in Sect. II, the relevant RMS delay spread can cause flat fading over a 40 MHz-wide channel. To cope with worst-case delay spread values, possible approaches are using: *i*) a single-carrier modulated signal at lower bit rate, thus reducing bandwidth occupancy; *ii*) a multicarrier transmission scheme with channel estimation and equalization at the receiver. Channel's time-variability is not an issue as the coherence time (Sect. II) is at least 5 times longer than the packet duration: 100 µs at 10 Mb/s for 128-byte packet.

Hereafter, the effect of retransmissions when using mmW is analyzed. A meaningful performance metric for packet-based wireless system is the throughput provided to the upper layer, evaluated through the goodput (GP), which is the ratio between the payload data delivered in an error-free packet and the required transmission time [27]. We denote by N_b the packet size in bit, T_b the duration of a bit, Z the maximum number of retransmission attempts before packet dropping, T_W the waiting time between two consecutive transmissions. T_W includes several contributions [28]: *i*) the delay for switching the transceiver from TX to RX, T_{turn}; *ii*) data *ack* transmission time T_{ack}; *iii*) duration of the inter-frame space (IFS) T_{IFS}. T_W is about 1.2 ms in 802.15.4 since the standard, at 250 kb/s, sets T_{ack} = 0.352 ms (6-byte PHY header plus 5-byte MAC header and trailer) and T_{IFS} = 0.64 ms (long IFS for frames greater than 18 bytes) [29], while T_{turn} is 0.192 ms in [28]. The propagation delay of radio signals is negligible (0.33 µs for a 100-m link).

We first introduce the following events with the associated probabilities, where PER is the packet error rate, and we assume the independence of attempt's failure or success.

$$A_i = \{\text{attempt } i\text{th successful}\} \rightarrow \Pr\{A_i\} = 1 - PER$$

$$\hat{A}_i = \{\text{attempt } i\text{th unsuccessful}\} \rightarrow \Pr\{\hat{A}_i\} = PER$$

$$D_z = \left\{\begin{matrix}\text{packet delivered} \\ \text{in } z \text{ attempts}\end{matrix}\right\} = \hat{A}_1 \cap \hat{A}_2 \ldots \cap A_z \rightarrow \Pr\{D_z\} = PER^{z-1}(1-PER)$$

$$S_Z = \left\{\begin{matrix}\text{packet delivered} \\ \text{within } Z \text{ attempts}\end{matrix}\right\} = D_1 \cup D_2 \ldots \cup D_Z \rightarrow \Pr\{S_Z\} = 1 - PER^Z$$

Let now express in Eq. (11) the average goodput ($\overline{GP}$) as the ratio between the average delivered bits and the average transmission time ($\overline{T}_{tx}$), irrespective of whether transmission is successful or not [30]. Under the constraint of the packet retry limit, expressed by Z, the number of successfully delivered bits is no longer a fixed value. It is instead a binary random variable that takes the values: N_b if delivery succeeds, which happens with probability $\Pr\{S_Z\}$; 0 if delivery fails [30]. Now, we denote by $T'_z = z\,N_b T_b + (z-1)T_W$ the elapsed time when a packet is successfully delivered at the z th attempt, and by $T_z = T'_z + T_W$ the elapsed time when, after packet's successful delivery, the transmitter is also set ready for the transmission of the next one. The probability of both T'_z and T_z is $\Pr\{D_z\}$. The overall time spent when the transmission is unsuccessful is $T_Z = Z\,N_b T_b + Z\,T_W$, whose probability is $1 - \Pr\{S_Z\}$ (notice that both T_z and T_Z include the waiting time T_W between consecutive packet transmissions). The average TX time and goodput are thus given by Eqs. (12)-(13).

$$\overline{GP} = N_b \cdot \Pr\{S_Z\} \,/\, \overline{T}_{tx} \tag{11}$$

$$\begin{aligned}\overline{T}_{tx} &= \sum_{z=1}^{Z} T_z \cdot \Pr\{D_z\} + \Theta_Z \cdot \left(1 - \Pr\{S_Z\}\right) \\ &= \sum_{z=1}^{Z} z(N_b T_b + T_W)\, PER^{z-1}(1-PER) + Z(N_b T_b + T_W) PER^Z\end{aligned} \tag{12}$$

$$\overline{GP} = \frac{N_b \cdot (1 - PER^Z)}{(N_b T_b + T_W)\left[\sum_{z=1}^{Z} z \cdot PER^{z-1} \cdot (1-PER) + Z \cdot PER^Z\right]} \tag{13}$$

$$PER = 1 - (1 - BER)^{N_b} \tag{14}$$

The PER in Eq. (13) depends on the BER and, in the simplifying case of a stationary channel with independent "bit

error" events (e.g., obtained thanks to the use of an opportune interleaving scheme), can be expressed as in Eq. (14). In its turn, the BER depends on the energy-to-noise spectral density ratio E_b / N_0, on the adopted MCS and on the type of distortion introduced by the channel which can be either narrowband flat (e.g., with the customary distributions Rayleigh, Rice, Lognormal, etc.), or wideband frequency-selective. Figure 7 presents $\overline{GP}$ vs. BER, for an ARQ system with $Z = 8$ and the wait time T_W from 0 to 10 ms. From Fig. 7 it is clear that a link rate of about 2 Mb/s is ensured for $T_W \le 0.4$ ms and for $BER \le 10^{-4}$. Although in Fig. 7 the maximum number of allowed retransmissions is $Z = 8$, in most of cases, $Z = 3$ re-transmissions are enough for a successful packet delivery. The average latency $\overline{T}_{succ}$ of the wireless system is the average of the time T_z' required for the successful transmission of a packet, conditioned on the event S_Z, see Eq. (15), where we put $\Pr\{D_z \cap S_Z\} = \Pr\{D_z\}$:

$$\overline{T}_{succ} = \mathrm{E}\{T_z' | S_Z\} = \sum_{z=1}^{Z} T_z' \Pr\{D_z | S_Z\} = \frac{\sum_{z=1}^{Z} [zN_bT_b + (z-1)T_W] \Pr\{D_z \cap S_Z\}}{\Pr\{S_Z\}}$$

$$= \sum_{z=1}^{Z} [zN_bT_b + (z-1)T_W] PER^{z-1} \cdot \left(\frac{1 - PER}{1 - PER^Z} \right) \quad (15)$$

Figure 8 shows $\overline{T}_{succ}$ vs. BER, for the same ARQ system as in Fig. 7. Considering a reasonable value of $T_W = 0.4$ ms (actually, the migration to mmW-band enables the use of bit-rates much greater than the 802.15.4's 250 kb/s, so that both T_{ack} and T_{IFS} scale down, accordingly), from Fig. 8 it emerges that, with $BER \le 10^{-4}$, the average latency is 150 µs. In a worst-case of $Z = 3$ re-transmission limit, and for the same parameters as in Fig. 8, the maximum latency results $T_{succ,\max} = ZN_bT_b + (Z-1)T_W = 0.9$ ms, with an occurrence probability lower than 10^{-2}. These latency values well compare w.r.t. those reported in literature for state-of-the-art systems operating over tens of meters at 2.4 GHz and at few kb/s (60 ms for a multi-hop in [2], 10 ms for a single link). With reference to the PHY, [31] considers for a 802.11-compliant PHY a link delay of 1 ms. Hence, the latency contribution of a 60 GHz PHY is negligible compared to the latency due to the higher layers of the protocol stack, and lower than values obtained with sub-6 GHz technologies.

In case of a multi-hop network, the maximum node distance is obtained multiplying the maximum number of hops N_{hop} with the maximum distance of a single hop (see Sect. V). The number N_{hop} affects also BER and latency performance of the link between any two nodes of the network. According to what discussed in [32], under the hypothesis that nodes belonging to the network are equipped with a processor supporting a decode and forward technique in the digital domain, the BER after N_{hop} hops (BER_N) can be calculated as N_{hop} times the BER in a single hop, provided that BER is small enough. In Section V (Table II), the link budget is sized to guarantee $BER = 10^{-10}$. Therefore, the number of hops can grow up to a theoretical value of $N_{hop} = 10^6$ before the total BER value increases up to 10^{-4} and the communication performance in Figs. 7 and 8 start decreasing. Such a high value of N_{hop} is not possible due to latency constraints. The average latency $\overline{T}_{MH}$ of the multi-hop network is $\overline{T}_{MH} = N \cdot (\overline{T}_{succ} + T_{enc} + T_{dec})$ being $\overline{T}_{succ}$ the average latency for a successful transmission of a packet, whereas T_{enc} and T_{dec} are the times for encoding/decoding at each node. In this work, customary concatenated RS and convolutional encoding, as in [18], has been considered. Since $\overline{T}_{succ}$ from Fig. 8 is 150 µs, whereas the sum $T_{enc} + T_{dec}$ amounts to at least 1 ms using 32-bit industrial microcontrollers, as in [33], then $T_{MH} \sim N_{hop} \cdot (T_{enc} + T_{dec})$. Safety-critical industrial applications can have a maximum latency requirement T_{max} from few ms to several seconds [34]; then the number N_{hop} of hops is limited by $N_{hop} < T_{\max} / (T_{enc} + T_{dec})$. In summary, adopting mmW PHY there are not stringent limits on the maximum number of hops, since this limit will come mainly by the ratio between the latency requirements of the application and the latency for channel-coding algorithms on the selected industrial processor.

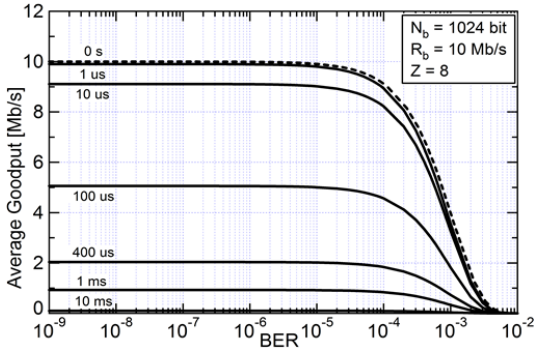

Fig. 7: $\overline{GP}$ vs. BER for a link with ARQ at different values of T_W

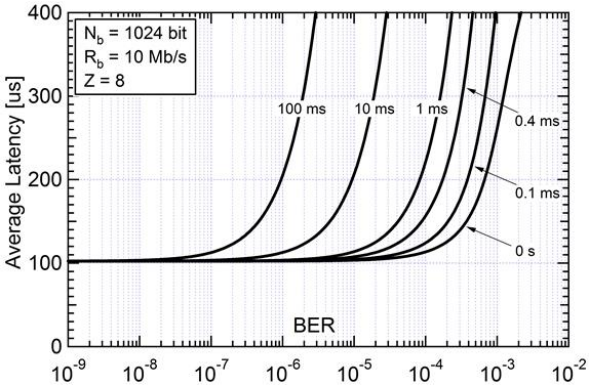

Fig. 8: $\overline{T}_{succ}$ vs. BER for a link with ARQ at different T_W values

VII. HW IMPLEMENTATION

This section discusses the feasibility at HW level of the techniques proposed in previous Sections, and the estimation of circuit complexity and power consumption of a node, whose bottlenecks are the mmW antenna and the transceiver. Low-cost technologies are considered: 65 nm CMOS SOI (silicon on insulator) for the integrated transceiver and PCB (Printed Circuit Board) using copper layer on RO4003 substrate for antennas and passive circuits. Some works [7, 35] for wireless networks at 60 GHz exploit a direct conversion scheme at TX side and homodyne demodulation at RX side.

Such architecture is limited to simple modulation techniques, e.g. On-Off Keying or Amplitude Shift Keying, and the 60 GHz oscillator is kept working at a fixed frequency since channel hopping techniques are not supported. To boost the performance of wireless industrial networks, at least QPSK is considered in Table II, and channel hopping at different frequencies is needed. To this aim, differently from [7, 35], in this work we adopt a double-conversion transceiver architecture (see Fig. 9), so that the frequency synthetizer should sustain multiple channels with a fast settling time but operating at around 30 GHz, a frequency halved vs. the 60 GHz of an homodyne scheme. For example, to support the 9 GHz range from 57 to 66 GHz, the synthetizer, working at halved frequency should generate signals from 28.5 to 33 GHz, with a step of 40 MHz and a settling time below 100 µs. At RX side in Fig. 9 a 60 GHz low noise amplifier (LNA) amplifies the received signal, which is mixed down to an intermediate frequency (IF) operating around 30 GHz.

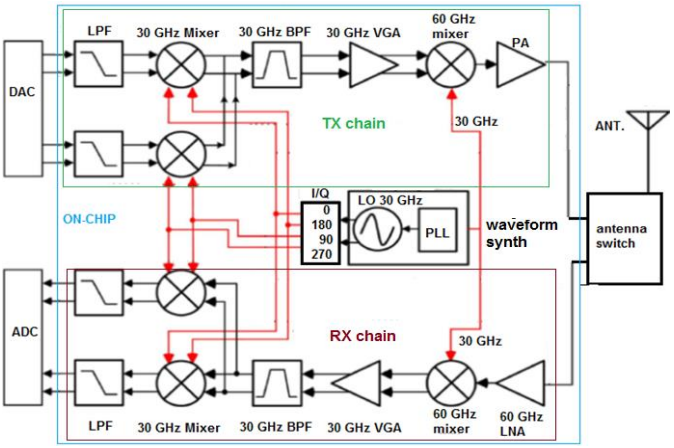

Fig. 9: Considered double conversion architecture

The LNA is a key block of the transceiver since, according to the Friis formula, the noise figure F of the whole receiving chain is the sum of the LNA noise figure, F_{LNA}, plus the noise contribution of the rest of the chain F_{rest} divided by the LNA gain G_{LNA}. 60 GHz mixers are known in literature determining a noise figure below 10 dB [36] for the RX stages following the LNA. Therefore, with an LNA gain of 15 dB, the noise figure F_{RX} of the whole receiver chain is de facto determined by the LNA noise figure. The 30 GHz IF signal is then amplified by a VGA (variable gain amplifier), bandpass filtered, and converted to a zero IF through a second mixer according to an I/Q demodulation scheme. The TX chain in Fig. 9 has a similar scheme. The key block is the power amplifier (PA), which provides a 10 dBm transmitted power. The key HW blocks (antenna, LNA, PA), have been designed from scratch. For the rest of the circuit, including the frequency synthetizer, we can implement the porting of the circuit in [26], for a 0.25 µm BiCMOS technology, to the 65 nm CMOS SOI technology. This technology features f_{max} and f_t performance higher than 150 GHz and hence it allows the same high frequency and fast settling times of the 0.25 µm BiCMOS in [26], but for a lower area and power consumption. This circuit allows a fast settling time below 1 µs, supporting the generation of the 40 MHz-wide channels, in the 57 GHz to 66 GHz range. Its power consumption is about 150 mW.

To implement the omnidirectional antenna considered in Section V, a co-planar patch antenna is used, which is printed, with a single copper layer, on a PCB board substrate, as in [37]. The antenna gain at 60 GHz is 1.44 dBi and varies from 1 dBi to 2 dBi along the 360 degrees of the XZ plane. When changing frequencies from 57 to 66 GHz, along the whole XZ plane, the gain varies from 0.8 dBi to 2 dBi. The area occupation of the omnidirectional antenna is 20 mm^2. Half-power beamwidth (HPBW) in the YZ plane is 75 degrees. For nodes needing a large FOV but not a full omni-directionality, e.g. yellow nodes in Fig. 2 in the mesh, the above antenna can be modified adding a reflecting conductive shield. This way the lobes in half of the plane are nulled, the beamwidth is limited from 360 degree to less than 180 degree, but the gain is increased up to a maximum of 5 dBi. Adopting other topologies, the beamwidth can be traded with the antenna gain. For example, in [38] a gain up to 8.7 dBi at boresight can be achieved with a 3-dB beamwidth of 72 degrees and a 10-dB beamwidth of 120 degrees over the 57–66-GHz band. In the scenarios considered in Table II, also high gain directive antennas are needed (e.g. yellow nodes in star topology). This antenna is implemented as a single array antenna, with a series of eight patches, printed using a single copper layer on a PCB. The maximum gain is 13.4 dBi with an HPBW of 20 degrees. The gain is at least 12 dBi in the 57 to 66 GHz range. The antenna area occupation is 12 mm^2 [39]. By increasing the array size to 32 patches, as in [40], organized as 8 parallel strings of 4 patches, the area increases to 600 mm^2, the gain is up to 18 dBi, the HPBW is 23 degrees and the bandwidth is 2 GHz. Even using a simple MCS, single-carrier QPSK with RS coding, with about 1 bit/Hz, the 2 GHz bandwidth ensures 20 times the maximum bit-rate required by industrial sensors, 10 Mb/s in Table II. In the 2 GHz bandwidth, the TSCH scheme is implemented with 50 channels, each 40 MHz wide.

For the PA, we designed in 65 nm CMOS SOI an amplifier consisting of 2 basic branches, each of them implemented as a cascade of two common source gain stages, with LC inter-stage matching. The output power of the two branches is combined through a Wilkinson combiner passive circuit. For the PA design, a circuit similar to that proposed for 5G in [35] has been used. The transistor widths in the 2 gain stages of each basic PA branch have been sized considering a current density of 0.3 mA/µm. Each single PA branch has an OP1dB (1-dB output power compression point) of 8.2 dBm. The whole PA (2 basic branches plus Wilkinson power combiner) has an OP1dB of 10.2 dBm. The area of the whole PA is 0.36 mm^2 whereas the efficiency is 11% (linear topology). To provide the 10 dBm at the antenna the PA power consumption is about 90 mW.

At RX side we designed in 65 nm CMOS SOI a 2 stage LNA, which ensures a gain of at least 15 dB for the whole 57-66 GHz range. The peak gain at 60 GHz is above 20 dB. The circuit topology is similar to that proposed in [36], although in this work the LNA input stage is sized to match the 50 Ω impedance of the off-chip antenna. The transistor widths in the 2 stages have been sized considering a current density of 0.15

mA/µm to optimize the noise figure. The LNA noise figure, which determines that of the whole RX chain, is below 5 dB for the 57 to 66 GHz range. The minimum is 4.5 dB at 60 GHz. The power consumption of the LNA is 23 mW and its area layout is 0.1 mm^2. The first LNA stage consists of a single-ended cascode stage, which provides a differential output signal to a fully differential second amplification stage through an integrated inter-stage transformer. The latter also provides the maximum power delivery from the first to the following stages of the LNA. The first LNA stage, in 65 nm CMOS SOI technology, has a peak gain of 10 dB. Its power consumption is 7 mW. This first stage is cascaded to a second stage consisting of a differential cascode amplifier, which is modified vs. classic solutions to remove common-source and common-gate stacked transistors, thus reducing the low-supply voltage issue. The inter-stage transformer between the two stages has been realized through two octagonal and symmetrical coupled planar inductors, both with 24 µm of diameter, one turns each, 3 µm spaced and 6 µm wide. The whole transceiver of Fig. 9, with a layout in 65 nm 1.2V CMOS SOI technology, has a power consumption in see Table IV of 120 mW for the TX chain (with the PA), 53 mW for the RX chain (with the LNA), and 115 mW for the waveform synthetizer (with the PLL). To reduce the energy consumption a power-down mechanism can be implemented, so the above power costs are paid only when the node is transmitting or receiving. The size of the nodes is limited by the area of the printed antenna on board with a maximum size of 6 cm^2 for high-gain patch antenna array.

TABLE IV. MMW TRANSCEIVER PARAMETERS IN 65 NM CMOS SOI

Power cons., mW			Die area	F_{RX}	OP1dB	Band, GHz
RX 53	TX 120	wave. syn. 115	2 mm^2	5 dB	10.2 dBm	57 to 66

VIII. CONCLUSIONS

This work investigates the potentiality of mmW as PHY in industrial wireless networks, proposing propagation, signal and noise models that consider harsh conditions such as multi-path, shadowing, NLOS, moving devices. The paper also discusses the efficient occupancy of the spectrum, the characterization of frequency-selective fading, the number of channels that can be provided and their bit-rate, the porting at mmW of TSCH and ARQ, the latency in single/multi-hop scenarios. With respect to sub-6 GHz links, the mmW PHY exploits worldwide multi-GHz free spectrum to increase link robustness by frequency-hopping and frequency-diversity. The achieved results in terms of distance, bit-rate, goodput, latency, number of channels and hops, power and area of the nodes, show the suitability of mmW PHY for industrial wireless networks at high bit-rate.

REFERENCES

[1] K.F.Tsang et al., "Industrial wireless networks: applications, challenges, and future directions," IEEE T. Ind. Inf., 12 (2): 755-75, 2016

[2] L. Ascorti et al., "A wireless cloud network platform for critical data publishing in industrial process automation," IEEE SAS2016, pp. 1-6

[3] H. Tung *et al.*, "The generic design of a high-traffic advanced metering infrastructure using ZigBee," IEEE T. Ind. Inf., 10 (1):836–844, 2014

[4] D. De Guglielmo, S. Brienza, G. Anastasi, "IEEE 802.15.4e: a Survey", Computer Communications, 88: 1-24, 2016

[5] Infineon Ag, "Single-chip 24 GHz radar front-end", Microwave J., 2014

[6] Infineon Ag, 24GHz Chipset-Family for Industrial Applications, Application note B132-H9722-G1-X-7600, Nov. 2012

[7] S. Saponara, et al., "Design exploration for millimeter-wave short-range industrial wireless communications", IEEE IECON 2016

[8] G.Athanasiou et al.,"Communication infrastructures in industrial auto mation: the case of 60 GHz mmW communications", IEEE ETFA 2013

[9] F. Giannetti, "Capacity evaluation of a cellular CDMA system operating in the 63-64-GHz band," IEEE Tr. on Vehic. Techn., 46 (1):55-64, 1997

[10] A. Maltsev et al., "Statistical channel model for 60 GHz WLAN systems in conference room environment," Radioengin., 20 (2):409-422, 2011

[11] Millimeter Wave Propagation: Spectum Management Implications," FCC, Office of Engineering and Technology, Bulletin n. 70, July, 1997

[12] P. Smulders, "Statistical characterization of 60-GHz indoor radio channels," IEEE T. Antennas and Propagation, 57 (10):2820-2828, 2009

[13] C. Gustafson, *60 GHz wireless propagation channels: characterization, modeling and evaluation*, Ph.D. Thesis, Lund University, 2014

[14] T.S. Rappaport, et al., "Wideband millimeter-wave propagation measurements and channel models for future wireless communication system design," IEEE Tr. on Comm., 63 (9): 3029-3056, 2015.

[15] S. Khademi, et al., "Channel measurements and modeling for a 60 GHz wireless link within a metal cabinet," IEEE Tr. Wir.Comm., 14 (9), 2015

[16] O. Hohlfeld et al., "Packet loss in real-time services: markovian models generating QoE impairments", IEEE IWQoS 2008, pp. 239-248

[17] M. Fakharzadeh, S. Jafarlou, A. Tabibiazar, "Indoor Multipath Measurements at 60 GHz," IEEE APSURSI, 2014

[18] B. Sklar, "Rayleigh Fading Channels in Mobile Digital Communication Systems Part I: Characterization," IEEE Comm. Mag., 1997, pp. 90-100

[19] S. Deng, et al., "28 GHz and 73 GHz millimeter-wave indoor propagation measurements and path loss models," IEEE ICC 2015

[20] T.S. Rappaport, Wireless Communications, *Prentice Hall*, 2002

[21] V. Degli-Esposti, et al., "Performance evaluation of space and frequency diversity for 60 GHz wireless LANs using a ray model," IEEE VTC'97

[22] H.-X. Zheng, "A model of 60 GHz indoor radio channel," Int. Journal of Infrared and Millimeter Waves, 24 (11): 1861-1873, 2013

[23] D. Dardari, et al., "Wideband indoor communication channels at 60 GHz," IEEE PIMRC'96, pp. 791–794

[24] *Digital Video Broadcasting; Implementation guidelines for DVB terre strial services; Transmission aspects*, ETSITR101190 V1.1.1 (1997-12)

[25] C. LeBlanc, "The future of industrial networking and connectivity", Industrial Ethernet Book, n. 2, 2015

[26] J. Lee et al., "A 28.5–32-GHz fast settling multichannel PLL synthesizer for 60-GHz WPAN radio," IEEE T. Mic. Theory and Tech., 56 (5), 2008

[27] D. Qiao et al.,, "Goodput analysis and link adaptation for IEEE 802.11a wireless LANs", IEEE T. Mobile Computing, 1 (4): 278-292, 2002

[28] G. Anastasi, et al., "A comprehensive analysis of the MAC unreliability problem in IEEE 802.15.4 wireless sensor networks," IEEE Tr. on Industrial Informatics, 7 (1): 52-65, 2011

[29] IEEE Std 802.15.4a™-2007.

[30] D. Qiao, et al., "Goodput analysis and link adaptation for IEEE 802.11a Wireless LANs," IEEE Tr. on Mob. Comp., 1 (4): 278-292, 2002

[31] A. Willig et al., "Measurements of a wireless link in an industrial environment using an IEEE 802.11-compliant physical layer," IEEE T. Ind. Elec., 40 (6): 1265-1282, 2002

[32] L. Couch, *Digital and analog communication systems*, Pearson, 2013

[33] Kan Yu et al., "Reliable and low latency transmission in industrial wireless sensor networks", Procedia Computer Sc., 5: 866-873, 2011

[34] M. Weiner et al., "Design of a low-latency, high-reliability wireless communication system for control applications", IEEE ICC2014

[35] S. Saponara, et al.,"Design exploration of mm-Wave integrated transceivers for short-range mobile communications towards 5G", Journal of Circuits Systems and Computers, 26 (4): 1-24, 2017

[36] M. Ercoli et al., "A passive mixer for 60 GHz applications in CMOS 65nm technology," IEEE German Microwave Conf., pp. 20-23, 2010

[37] S. Ranvier et al., "Low-cost planar omnidirectional antenna for mm-wave applications," IEE Antennas and Wireless Prop. Lett., 7, 2008

[38] A. Amadjikpè, et al., "Integrated 60-GHz antenna on multilayer organic package with broadside and end-fire radiation", IEEE T. Microwave Theory and Tech., 61 (1):303- 315, 2013

[39] J. Säily et al., "Low cost high gain antenna arrays for 60 Ghz millimeter wave identification," ESA Worksh.on Mill.-Wave Tech. and App., 2011

[40] C. Karnfelt et al., "High gain active microstrip antenna for 60-GHz WLAN/WPAN applications," IEEE T. Micr. Theory Tech., 54 (6), 2006